# Atomic structures of supersaturated ZnO–Al$_2$O$_3$ solid solutions

Satoru Yoshioka,[a)] Fumiyasu Oba, Rong Huang, and Isao Tanaka[b)]
*Department of Materials Science and Engineering, Kyoto University, Sakyo, Kyoto 606-8501, Japan*

Teruyasu Mizoguchi
*Institute of Engineering Innovation, The University of Tokyo, Bunkyo, Tokyo 113-8656, Japan*

Tomoyuki Yamamoto
*Department of Materials Science and Engineering, Waseda University, Shinjuku, Tokyo 169-8555, Japan*

Supersaturated ZnO–Al$_2$O$_3$ (>20 at. % Al) thin films are grown by pulsed laser deposition technique on silica glass substrates at 600 °C. They are characterized by combining x-ray diffraction, Al-$K$ edge x-ray absorption near edge structures (XANESs), high resolution transmission electron microscope (TEM) imaging, TEM analysis, and a series of first principles calculations. The films are composed of textured wurtzite grains with $c$ planes parallel to the substrate. The distance between $c$ planes expands significantly when the Al concentration is greater than 10 at. %. The expansion disappears after annealing the films at above 800 °C. High density of dislocationlike defects is found in the as deposited film. Any segregation of Al cannot be detected either at the grain boundaries or inside the grains. The lattice expansion toward $c$ axis and the experimental XANES can be satisfactorily explained by taking a hypothetical homologous model with the composition of $(ZnO)_3(Al_2O_3)$ as the local environment of Al in the supersaturated solid solution. Simplified substitutional models with Al at the Zn site in wurtzite ZnO cannot explain these experimental results. First principles calculations show that the homologous phase is energetically more favorable than the simplified substitutional models, although decomposition into ZnO and ZnAl$_2$O$_4$ is more favorable than the homologous phase. The local atomic structures of the supersaturated solid solution are therefore concluded to be analogous to the metastable homologous phase. © *2008 American Institute of Physics*. [DOI: 10.1063/1.2829785]

## I. INTRODUCTION

Many kinds of wide-gap materials are synthesized in thin films through chemical or physical deposition routes. They are typically made at lower temperatures than those required by a conventional solid-solid reaction route. Materials obtained in such ways are often metastable from thermodynamical viewpoint. High doping levels beyond solubility limit under thermal equilibrium or "supersaturated solid solutions" can often be obtained. In many cases, however, they are not recognized as metastable or supersaturated. In fact, quantitative information of equilibrium solubility limits is known only in limited systems.

Since dopants act as functional centers, information of their local atomic/electronic structures is very important. In dilute solid solutions, a dopant atom may be treated as isolated from the other defects. In concentrated solid solutions, which are often supersaturated, interactions among dopants and point defects such as vacancies should not be neglected.[1–3] Systematic works by combining x-ray absorption near edge structure (XANES) or near edge x-ray absorption fine structure (NEXAFS) and first principles calculations have been made recently in the present authors' group.[4–9] XANES provides complementary information to the other techniques such as x-ray diffraction, since it monitors the

local environment of selected elements. Samples need not to be large crystals. They can be either amorphous, highly distorted, or nanosized crystals.

In the present study, we investigate the local structure of Al solute atoms in ZnO. Samples are concentrated solid solutions synthesized by pulsed laser deposition (PLD) technique. They are characterized by transmission electron microscopy (TEM), x-ray diffraction (XRD), and XANES. First principles calculations are systematically made to evaluate the local structures and energetics. Theoretical XANES is also obtained by first principles calculations.

ZnO–Al$_2$O$_3$ system is selected in the present study, first because of the engineering importance of Al-doped ZnO as an $n$-type transparent electric conductor.[10,11] Second, the crystal structure of ZnO is wurtzite (space group: $P6_3mc$), which is relatively simple and therefore suitable for detailed fundamental study. Although many works have already been made for ZnO doped with dilute Al, no systematic work can be found in literature for the concentrated solid solutions with Al contents more than 5 at. % (note that at. % in the present study always refers to cation%). No XANES works of the ZnO–Al$_2$O$_3$ alloys have been reported, either. The reason is simple. ZnO–Al$_2$O$_3$ solid solutions typically show highest electric conductivity when Al content is in between 1 and 5 at. %. The conductivity decreases dramatically with further increase of the Al content. Researchers have not paid much attention to concentrated ZnO–Al$_2$O$_3$ alloys with poor

[a)]Electronic mail: syoshioka@nucl.kyushu-u.ac.jp.
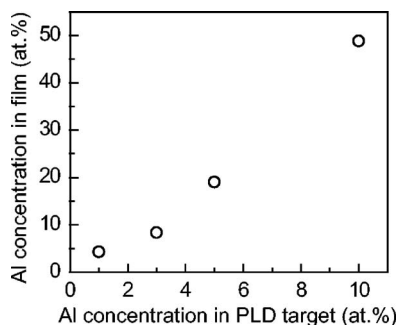[b)]Electronic mail: tanaka@cms.mtl.kyoto-u.ac.jp.

FIG. 1. Relationships between the Al concentration of PLD thin films and that of PLD targets measured by SEM-EDS.

electric conductivity. However, the fundamental knowledge of such systems should be important for wider application of these alloys.

## II. EXPERIMENTAL PROCEDURE

The $ZnO-Al_2O_3$ samples have been synthesized in two ways. Two starting powders, $\alpha$-$Al_2O_3$ (AKP-30, Sumitomo Chemicals) and ZnO (Seido Chemicals), were mixed in ethanol using magnetic stirrer until they dried up. The mixed powder was cold isostatically pressed at 100 GPa and then sintered in air at 1350 °C for 3 h, followed by furnace cooling with the rate of 200 °C/h. The samples made in this way will hereafter be called "ceramic samples." A $ZnAl_2O_4$ sample as a reference was made in the same way as the ceramic samples.

Thin film samples were prepared by PLD technique using an excimer KrF* laser source ($\lambda = 248$ nm, $\tau = 25$ ns, Lambda physik COMPex205). Laser frequency was kept at 10 Hz. The ceramic samples were used for the targets of PLD. Laser power was approximately $3 \times 10^4$ J/m$^2$. All PLD experiments were made in oxygen backfill pressure of $p_{O_2} = 0.3$ Pa. High purity $SiO_2$ glass plates were used as substrates. Substrate temperature was 600 °C.

It should be noted that the composition of the PLD film is not always the same as that of the target. According to Choopun *et al.*[12] Zn-related species have a higher vapor pressure and thereby easily desorbed at higher growth temperature during the PLD of ZnO–MgO. They found that the composition of MgO increases almost linearly with the substrate temperature, although the film grown at room temperature shows a composition very close to the target. In the present study, the composition was determined via energy dispersive x-ray analysis (EDS) of the film using a scanning electron microscopy (SEM) and a transmission electron microscopy (TEM). The SEM data were supplied for the ZAF correction. The TEM data were quantified in the thin film limit. Inductively coupled plasma atomic emission spectroscopy (ICP-AEP) analyses have also been made for cross-check. Samples for ICP firstly soaked into hydrochloric acid. Then nitrate acid was added to completely dissolve the thin film before the analysis. The mixture of acid did not dissolve the glass substrate. The results of the chemical analyses by SEM-EDS are shown in Fig. 1. The Al concentration in the PLD film is higher by a factor of 3–5 than that of the target.

The relationship between target composition and film composition is not linear. The volatility of film constituents may be dependent on the composition.

All samples were investigated by XRD using Cu $K\alpha$ radiation and conventional $\theta$-$2\theta$ scan (Rigaku, RINT 2000). XANES spectra were obtained at BL1A beamline of UV-SOR (Okazaki, Japan) by total electron yield method (TEY) using an electron multiplier. The beamline is equipped with a focusing premirror and a double crystal monochromator. The KTP (110) was used as an analyzing crystal for the monochromator. All measurements of XANES spectra were carried out in vacuum of $1 \times 10^{-4}$ Pa at room temperature. Thin film samples were set with its surface 50° to the incident x-ray beam. The angle is close to $\cos^{-1}(1/\sqrt{3}) = 54.7°$, which should provide averaged XANES of all crystallographic directions.[13] Samples were mounted using adhesive carbon tapes. No surface coating to avoid charging was found to be necessary. TEM samples were made by a standard technique including slicing, dimpling, and ion milling. Observations were made using a TEM equipped with a field emission type electronic gun (Philips CM200FEG).

## III. COMPUTATIONAL PROCEDURE

First principles band-structure calculations have been made using two kinds of methods. One is the projector-augmented wave (PAW) method[14] as implemented in the VASP code.[15] This makes efficient and accurate optimization of atomic arrangements and evaluation of total energies. The exchange-correlation term was treated with the generalized gradient approximation (GGA) as formulated by Perdew, Becke, and Enzerhof (PBE).[16] Monkhorst-Pack $k$-point grid[17] with a spacing of ~0.4 Å$^{-1}$ was used for all structures. The kinetic energy cutoff for the plane wave basis was 500 eV for all calculations. Structural optimization was truncated when the forces on all ions and the stress became $<2.0 \times 10^{-3}$ eV/Å and $<5.0 \times 10^{-2}$ GPa.

In order to obtain theoretical XANES correctly, it is necessary to take into account the correlation between the core hole and the excited electron. It can be evaluated in a straightforward way using all electron methods. For this purpose, we have employed the other theoretical method, i.e., the full-potential linearized augmented plane wave plus local orbital (FLAPW+lo) technique as implemented in WIEN2K code.[18] The muffin-tin radius $R_{MT}$ was set to 0.86 Å for all atoms. The product of the muffin-tin radius and the maximum reciprocal space vector $K_{max}$, i.e., the plane wave cutoff, $R_{MT}K_{max}$, was fixed at 3.1 Å eV$^{1/2}$ (6.0 bohrs Ry$^{1/2}$). Theoretical XANES spectra were calculated within the electronic-dipole transitions. The core-hole effects were taken into account by removing one electron on Al $1s$ orbital of interest and putting one additional electron at the bottom of the conduction band. In order to avoid the artificial interactions among core holes, supercell sizes were chosen to be more than 100 atoms. Each of calculated spectra was broadened by the Gaussian function of 1.0 eV full width at half maximum. Transition energies were obtained as the difference in total energy between the ground and core-hole states.
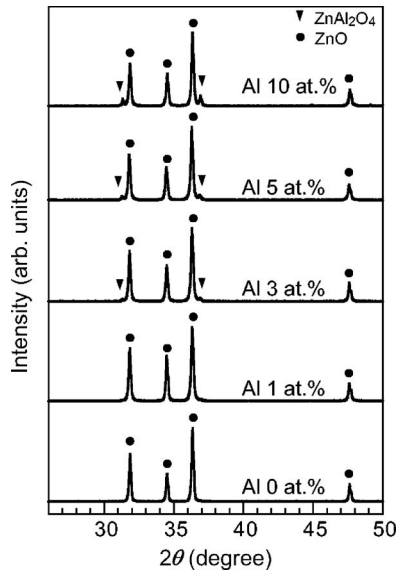
FIG. 2. XRD profiles by $\theta$-$2\theta$ method of ZnO$-$Al$_2$O$_3$ ceramic samples fired at 1350 °C for 3 h. The circles and triangles denote the peaks assigned to those of ZnO and ZnAl$_2$O$_4$, respectively.

More details of the XANES calculations can be found elsewhere.[19]

## IV. RESULTS

### A. Characterization of ceramic samples

We firstly investigate the series of ZnO$-$Al$_2$O$_3$ ceramic samples with Al contents of 1, 3, 5, and 10 at. %. Figure 2 shows the XRD profiles of four samples. Presence of ZnAl$_2$O$_4$ (space group: $Fd\bar{3}m$) with a spinel structure can be found in samples with Al contents of more than 3 at. %. No XRD peaks of ZnAl$_2$O$_4$ can be detected in the 1 at. % Al sample even when the intensity of XRD peaks is displayed in a logarithmic scale. Figure 3 shows Al-$K$ edge XANES of the samples with Al contents of more than 3 at. %, together
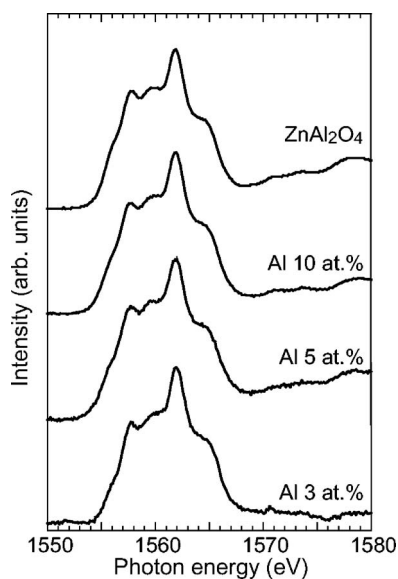


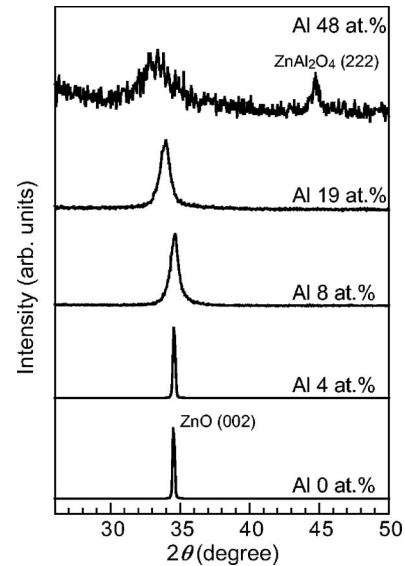FIG. 3. Al-$K$ edge XANES spectra of ZnO$-$Al$_2$O$_3$ ceramic samples fired at 1350 °C for 3 h, together with that of ZnAl$_2$O$_4$ as a reference.



FIG. 4. XRD profiles by $\theta$-$2\theta$ method of ZnO and ZnO$-$Al$_2$O$_3$ films as deposited at 600 °C.

with that of ZnAl$_2$O$_4$ as a reference. The spectral shape of 3 at. % Al sample is nearly the same as those of the higher doped samples, and also of ZnAl$_2$O$_4$. We were unable to measure the Al-$K$ edge XANES from the 1 at. % Al sample with sufficient signal to background ratio in the present experimental setup.

Two things can be learned from these two experimental results: (1) The Al-$K$ edge XANES of the ceramic samples exhibits *fingerprint* of ZnAl$_2$O$_4$. The positions and intensities of the peaks, including small ones, are nearly identical with those in the ZnAl$_2$O$_4$ spectrum. The local environment of the major part of Al atoms in these samples is, therefore, likely to be similar or identical to that in ZnAl$_2$O$_4$. This will be further confirmed by first principles calculations in this paper (Fig. 14). (2) The solid solubility of Al in ZnO under the present experimental conditions is less than 3 at. %. Above the solubility limit, phase separation to ZnO:Al and ZnAl$_2$O$_4$ should take place. Al-$K$ edge XANES can discriminate Al atoms in different environments, whereas XRD measures only relative amounts of different crystalline phases. Assuming that the solubility is 2 at. % Al, the XRD of the 3 at.%Al sample can be given by the superposition of ZnO:Al and ZnAl$_2$O$_4$ with a ratio of 63.7: 1. On the other hand, the ratio
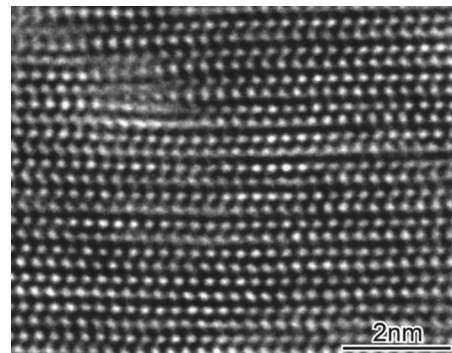


FIG. 5. Cross sectional high-resolution TEM image of the as deposited ZnO$-$Al$_2$O$_3$ film with 19 at. % Al.
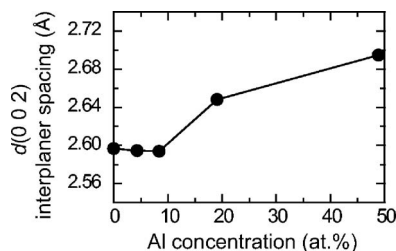
FIG. 6. Interplanar distances of wurtzite (002) for the as deposited ZnO and ZnO–Al₂O₃ films obtained from XRD shown in Fig. 4. Experimental errors are smaller than the diameter of the data point circles.

for XANES is 1.9:1, since the $ZnAl_2O_4$ phase contains 33.3 times more Al than the ZnO–2 at. % Al phase. The sensitivity to detect $ZnAl_2O_4$ is roughly 30 times better in XANES. The solubility limit of Al in ZnO was reported by Yoon *et al.*[20] using XRD and Raman spectra on samples synthesized at 1300 °C × 5 h. They have concluded that the solubility limit is 2 at. % Al. The present study uses much sensitive technique to find the solubility limit in the same range under these experimental conditions.

## B. Characterization of PLD thin films as deposited

Four doped and one undoped ceramic samples were used as PLD targets. As shown in Fig. 1, the Al concentrations of the PLD films are three to five times greater than those of the targets. We will hereafter use the measured Al concentrations to denote these PLD films. Figure 4 shows the XRD of five samples deposited on SiO₂ glass substrates. PLD of undoped ZnO on the SiO₂ glass has been known to produce a textured ZnO film with *c* planes parallel to the substrate.[21] In agreement with the literature work, a single peak corresponding to wurtzite ZnO (002) reflection can be seen in the undoped sample. Doped samples with 4–19 at. % Al also display single XRD peaks. The peak position clearly shifts to the
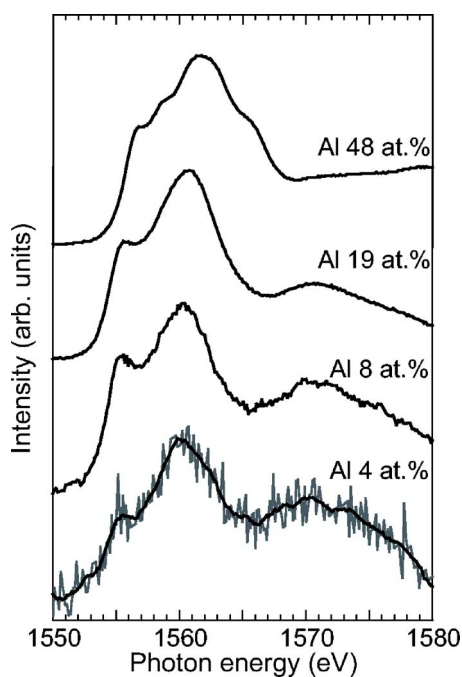


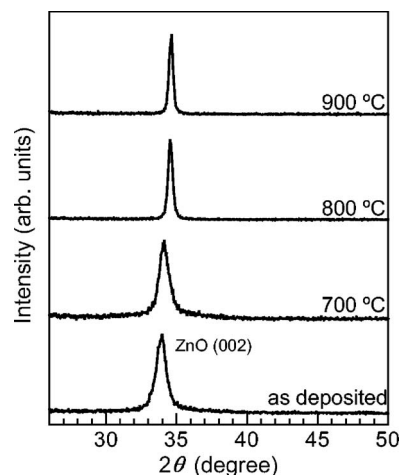FIG. 7. (Color online) Al-*K* edge XANES spectra of the as deposited ZnO-Al₂O₃ films.



FIG. 8. Changes in XRD profiles of the 19 at. % Al ZnO–Al₂O₃ film with annealing temperature after the deposition.

lower angle when the concentration of Al is greater than 10 at. %. At the same time the peak intensity decreases by two orders of magnitude, and the peak width increases significantly, as can be seen in Fig. 4.

The microstructure of the highly doped thin film was examined by cross sectional TEM technique. The PLD film thickness is evaluated to be 200 nm. The sample is composed of wurtzite ZnO:Al grains, and the *c* planes of these grains are almost parallel to each other. Typical grain diameter parallel to the film surface is a few 10 nm. No secondary phases can be found. Figure 5 shows a high resolution image of the 19 at. % Al sample. Within the grain, high density of dislocationlike atomic structures is observed. Any segregation of Al cannot be detected either at the grain boundaries or inside the grains using TEM-EDS with electron-beam spot size of 1 nm. We can therefore ascribe the XRD peak of the 19 at. % Al sample to the ZnO(002) reflection as in the case of the undoped sample.

The interplanar distance of (002), i.e., $d(002)$ can be determined from the XRD peak position following a standard procedure composed of the $K\alpha_2$ removal and the fitting to a Gaussian function. The results are plotted in Fig. 6 as a function of the Al content. $d(002)$ of undoped ZnO in the present sample is 2.60 Å, which is very close to that in the JCPDS file,[22] i.e., 2.603 and 2.602 Å. As can be seen in Fig. 6, $d(002)$ is almost unchanged up to 8 at. % doped samples. Further increase in the Al content brings about significant increase in $d(002)$. The origin of the decrease and increase in
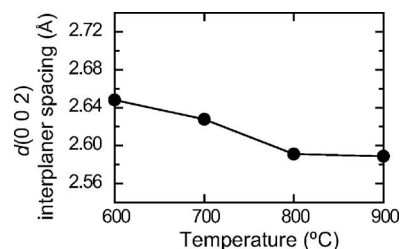


FIG. 9. Changes in the interplanar distances of wurtzite (002) with annealing temperature in the 19 at. % Al ZnO–Al₂O₃ film. Experimental errors are smaller than the diameter of the data point circles.
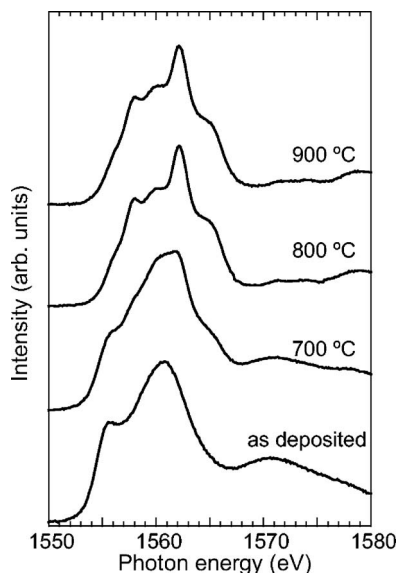
FIG. 10. Changes in Al-*K* edge XANES spectra of the 19 at. % Al ZnO−Al$_2$O$_3$ film with annealing temperature.
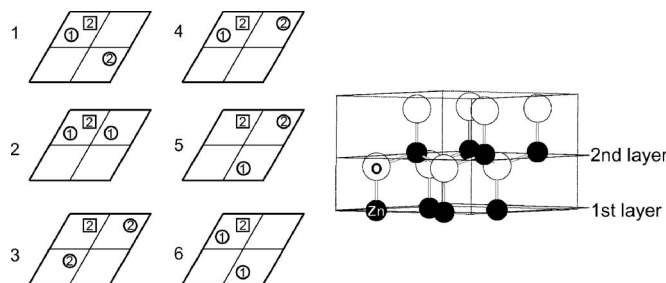


FIG. 11. Solutes and vacancy configurations in ZnO:Al substitutional alloys for the Zn-vacancy models. Six different ways can be made to put two Al (○) and one vacancy (□) in the eight-cation-site cell with two cation *c* planes. The numbers 1 and 2 correspond to the first and second layers of the cation *c* planes (left panel, viewed from the direction parallel to the *c* axis; right panel, viewed from a direction normal to the *c* axis).

the interplanar spacing will be discussed later with the information obtained by first principles calculations.

Al-*K* edge XANES of four samples are shown in Fig. 7. Unfortunately, the quality of the XANES of the 4 at. % Al is poor. Smoothing operation using Savitzky-Golay algorithm[23] was carried out for the spectrum. Comparison of Figs. 3 and 7 can find that the Al-*K* edge XANES of 4, 8, and 19 at. % Al films do not exhibit fingerprint of ZnAl$_2$O$_4$. Although the constituent peaks are much broader than those in the ZnAl$_2$O$_4$ spectrum, clear differences can be found in their positions and intensities. It should correspond to Al atoms in the supersaturated solid solution. The atomic environment corresponds to the XANES will be discussed later in this paper with the aid of theoretical fingerprints of XANES (Fig. 14). The XANES of 48 at. % Al film is different from those of lower Al content samples. This can be interpreted as the superposition of two spectra from ZnAl$_2$O$_4$ and the supersaturated solid solution. This will also be explained in the next chapter.

### C. Characterization of PLD thin films after heat treatments

The present PLD films were deposited at 600 °C. In order to examine the phase separation process, the PLD samples were treated at 700, 800, and 900 °C for 3 h in the flow of the mixture of gas (80% Ar+20% O$_2$). Figure 8 shows XRD profiles of the 19 at. % Al sample after the heat treatments. No extra peak appears by the heat treatment. The peak width is found to decrease significantly. Figure 9 shows *d*(002) evaluated by the XRD. A clear decrease in *d*(002) can be recognized. After annealing at 800 °C, *d*(002) reaches the value of the Al-doped ceramic samples and the as deposited 4 and 8 at. % Al films. Further increase in the annealing temperature up to 900 °C does not change *d*(002).

Evolution of Al-*K* edge XANES of the 19 at. % Al film with heat treatments is shown in Fig. 10. Samples annealed above 800 °C show clear fingerprint of ZnAl$_2$O$_4$. The spec-

trum of the 700 °C annealed sample can be ascribed to the superposition of the spectra of ZnAl$_2$O$_4$ and the supersaturated solid solution. Combining the information obtained by the XRD results, phase separation of the supersaturated solid solution to thermal equilibrium phases, i.e., ZnAl$_2$O$_4$ and ZnO:Al at the solubility limit, is implied to occur during the heat treatments. The absence of ZnAl$_2$O$_4$ phase in the XRD profile after the heat treatment can be ascribed to tiny crystallite size or poor crystallinity of the ZnAl$_2$O$_4$ precipitates.

## V. DISCUSSION

### A. Origin of lattice expansion

In the previous chapter, we have reported the formation of the supersaturated ZnO−Al$_2$O$_3$ with more than 10 at. % Al by the PLD process. The *d*(002) spacing was found to increase when the Al content is greater than 8 at. % (Fig. 6). Similar expansion was reported in ZnO−Al$_2$O$_3$ films by Mass *et al.*[24] They made a series of films on sapphire substrates by PLD using KrF* laser with O$_2$ pressure of 0.13 Pa and substrate temperature of 750 °C. The *d*(002) spacing was found to increase by 1.5%–1.9% when the Al concentration of the target was greater than 3 at. %. Although they did not report the real Al content of the film, it should be more than five times greater than that of the target since their deposition temperature is 150 °C higher than the present one. The present results should be consistent with their results when the Al content of their samples is corrected.

In order to elucidate the origin of the lattice expansion toward the *c* axis, a series of first principles calculations were made using the PAW method. When Al solutes substitute for the cation site of ZnO, two kinds of defect equations can be thought. One is the *n*-type conductor model with Al$_{Zn}^{\cdot}$+*e*′, which occurs in dilute alloys. This will be hereafter called *n*-type model. In the second model the extra charge is compensated by the formation of Zn vacancies as Al$_{Zn}^{\cdot}$+1/2 V$_{Zn}$″. The latter model will be called Zn-vacancy model. Although the supersaturated solid solution with high Al content may be better described by the Zn-vacancy model, we made first principles calculations for these two cases for comparative discussion. The supercell for the *n*-type model is composed of 128 atoms with one cationic site substituted by an Al atom. For the Zn-vacancy model, we have adopted a su-

TABLE I. Lattice parameters and volume of six Zn-vacancy models for $ZnO-Al_2O_3$ shown in Fig. 11. Relative energies $\Delta E$ per $Zn_5Al_2O_8$ are shown together.

| | Lattice parameter (Å) | | | Volume (Å$^3$) | $\Delta E$ (eV) |
|---|---|---|---|---|---|
| | $a$ | $b$ | $c$ | | |
| 1 | 3.20 | 3.20 | 5.21 | 186 | $\cdots$ |
| 2 | 3.22 | 3.16 | 5.27 | 187 | 0.72 |
| 3 | 3.28 | 3.28 | 5.16 | 188 | 0.51 |
| 4 | 3.22 | 3.30 | 5.15 | 188 | 0.35 |
| 5 | 3.24 | 3.31 | 5.09 | 188 | 0.93 |
| 6 | 3.27 | 3.27 | 5.20 | 188 | 1.26 |

percell of wurtzite structure composed of eight cationic and eight anionic sites. Two of cationic sites were made to be occupied by Al. A Zn vacancy was then generated. The formula unit of the supercell is thus given by $Zn_5Al_2O_8$. A geometry analysis can find six different ways to put two Al and one Zn vacancy in the eight-cation-site cell. They are summarized in Fig. 11. First principles calculations were made for all of these six configurations allowing relaxation of unit cell dimensions and atomic positions.

The lattice parameters obtained for these models are listed in Table I. The deviations in the angles between the lattice vectors $a$, $b$, $c$ from the hexagonal values are less than 2°. Theoretical cell parameters of wurtzite ZnO ($w$-ZnO) are $a=3.28$ Å and $c=5.31$ Å, which are +1.3% and +2.1% greater than those by experiment. The error is typical for first principles calculations with the GGA. As compared to the pure $w$-ZnO, none of these models shows expansion of the cell toward the $c$ axis. It should be noted that the coordination number (CN) of Al atoms in these models are always 4 even after the structural optimization.

The fact that the lattice expansion cannot be explained by a simple substitutional model with CN=4 implies that the solute Al atoms are located in different local environments. A candidate structure can be given from the analogy to the $ZnO-In_2O_3$ system. They are known to form a series of ordered structures known as homologous phases $(ZnO)_m(In_2O_3)$, where $m$ is an integer with $m \geqslant 3$.[25–29] Al-though homologous phases have not been reported for the $ZnO-Al_2O_3$ system, it may be present as a metastable structure.

In the present study, a model of a homologous phase with the composition of $(ZnO)_3(Al_2O_3)$ is examined using experimental $(ZnO)_3(In_2O_3)$ homologous structure ($R\bar{3}m$) as a prototype.[30] The structure of the homologous $(ZnO)_3(Al_2O_3)$ optimized in the present calculation is given in Fig. 12. The prototype $(ZnO)_3(In_2O_3)$ homologous structure is composed of ZnO layers sandwiched in $In_2O_3$ layers. In order to maintain the charge neutrality, some Zn atoms in the ZnO layers are substituted by In atoms. The In atoms in the $In_2O_3$ layer has CN=6. On the other hand, the In atoms substitutionally present in the ZnO layers show CN=4 or 5. There is an ambiguity associated with the location of the In atoms in the ZnO layers. In the present study, we have chosen a representative structure, which is shown in Fig. 12. As can be found, the ZnO layers in the homologous structure are analogous to the layers in $w$-ZnO except for the presence of the CN=5 Al atoms. The corresponding interplanar distances range from 2.71 to 2.99 Å in the homologous phase, which is 2.3%–12.7% larger than the $d(002)$ of the $w$-ZnO, i.e., 2.65 Å. It is interesting that the interplanar distances around the CN=6 Al atoms are 2.99 Å, which is 12.7% larger than that of $w$-ZnO. The experimental $d(002)$ of $w$-ZnO expands by 2.0% and 3.8% with 19 at. % Al and 49 at. % Al, as
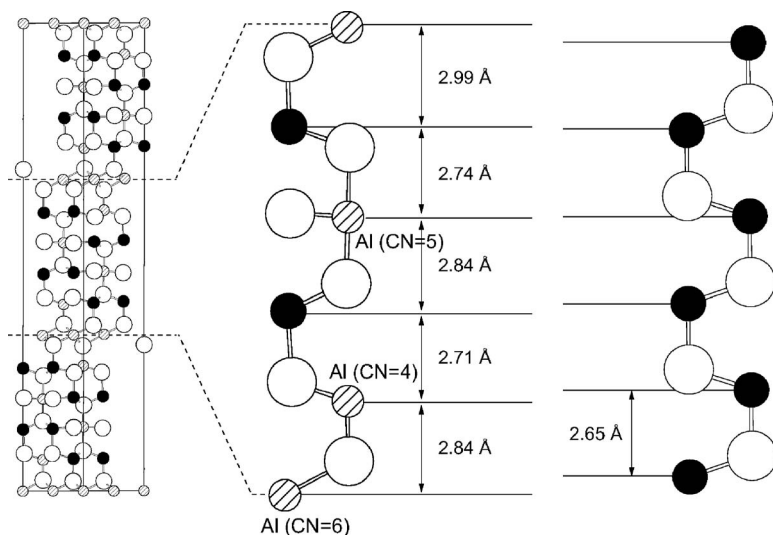


FIG. 12. Theoretical structure of the homologous $(ZnO)_3(Al_2O_3)$ after optimization by the first principles PAW calculation. Theoretical structure of the wurtzite ZnO optimized in the same way is shown for comparison.
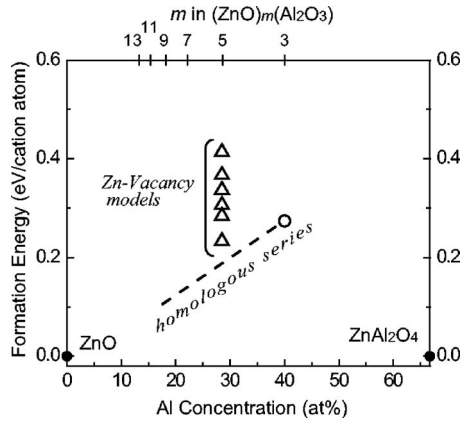
FIG. 13. Formation energy of the Zn-vacancy and homologous $(ZnO)_3(Al_2O_3)$ models for $ZnO-Al_2O_3$ relative to *w*-ZnO and $ZnAl_2O_4$ as computed by Eq. (1). The open triangles and circle denote six Zn-vacancy models and the homologous model, respectively.

shown in Fig. 6. The magnitude of the expansion in the supersaturated solid solution can be well explained by taking inclusion of Al of CN=5 or 6 into account.

## B. Formation energy of alloy models

The formation energy of alloy models shown in Table I and those of homologous phases are compared in Fig. 13. They are relative to *w*-ZnO and $ZnAl_2O_4$ as given by

$$\Delta E = E_t[(ZnO)_m(Al_2O_3)] - (m-1)E_t[ZnO] \\ - E_t[ZnAl_2O_4], \tag{1}$$

where $m=5$ for the Zn-vacancy model and $m=3$ for the present homologous model. $E_t$ is the total energy per chemical formula shown in the square bracket. The formation energy for the *n*-type model is not shown in Fig. 13 because it

varies with chemical potentials of constituents, as determined, for example, by the oxygen partial pressure. Its direct comparison with the formation energy of the other models may be confusing.

The formation energy of the alloy models are all positive values, which is consistent with the experimental results that the supersaturated solid solutions eventually decompose into the mixture of *w*-ZnO and $ZnAl_2O_4$. In the series of $(ZnO)_m(In_2O_3)$ homologous compounds, the thickness of the ZnO layer with In of CN=4 is known to increase with the decrease of the $In_2O_3$ content without changing the $In_2O_3$ layers. The formation energy of the homologous series $(ZnO)_n(Al_2O_3)$ $(n > 3)$ can therefore be roughly approximated by the line that connects *w*-ZnO and $(ZnO)_3(Al_2O_3)$, as displayed in Fig. 13. It is interesting that the line is located to be lower than the lowest formation energy of the Zn-vacancy model at the Al content of 28.6 at. % (=2/7). This implies that the homologous type structure with Al of CN =5 and 6 is energetically preferable to the Zn-vacancy model with Al of CN=4 when the Al content is high.

## C. Interpretation of Al-*K* edge XANES

The expansion toward *c* axis can be explained by the presence of Al in the CN=5 or 6 environment associated with the formation of homologous type structures. The formation of the homologous type structures is also suggested to be energetically more favorable than the Zn-vacancy model with Al only of CN=4. However, the formation of such an ordered structure has not been found by our x-ray diffraction investigation. Here we examine the experimental Al-*K* edge XANES with the aid of theoretical XANES obtained by first principles calculations. Figure 14 shows theoretical XANES of five models, i.e., (1) $\alpha$-$Al_2O_3$ (corundum),
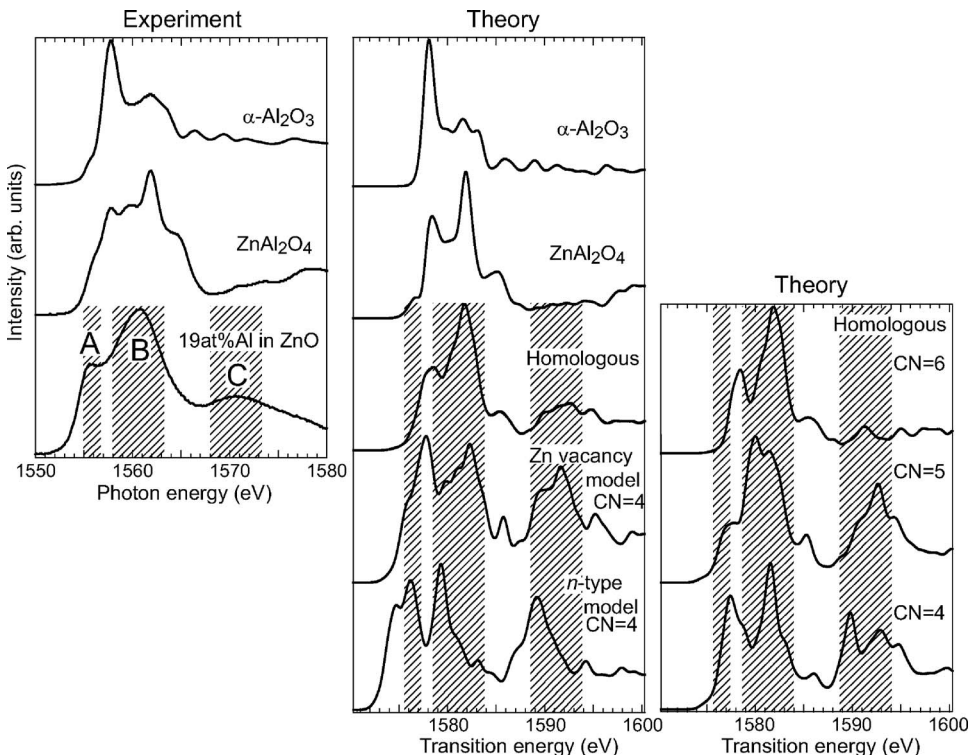


FIG. 14. (Left) Experimental Al-*K* edge XANES of $\alpha$-$Al_2O_3$, $ZnAl_2O_4$ and the 19 at. % Al $ZnO-Al_2O_3$ film. (Middle) Theoretical Al-*K* edge XANES of homologous $(ZnO)_3(Al_2O_3)$, Zn-vacancy, and *n*-type models for $ZnO-Al_2O_3$ together with those of $\alpha$-$Al_2O_3$ and $ZnAl_2O_4$. (Right) Theoretical Al-*K* edge XANES corresponding to three sites of Al with different coordination numbers (CNs) in the homologous $(ZnO)_3(Al_2O_3)$. The energy ranges for the three characteristic peaks, A, B, and C, in the experimental spectrum of the 19 at. % Al sample are hatched.

(2) ZnAl$_2$O$_4$ (normal spinel), (3) (ZnO)$_3$(Al$_2$O$_3$) homologous model, (4) Zn-vacancy model, and (5) *n*-type model. The size of supercell was 120 atoms for (1), 112 atoms for (2), 132 atoms for (3) and 120 atoms for (4), and 128 atoms for (5). For the homologous structure, three sets of calculations were independently made for three Al sites (CN=4, 5, and 6) as shown in the right panels of Fig. 14. They were summed up with weights of 1:1:2 to make the theoretical spectrum in the middle panel. For the Zn-vacancy model, the model 1 in Table I was selected, which is energetically most favorable. The energy scale of the theoretical spectra was translated by 20.4 eV in order to adjust the peak position of $\alpha$-Al$_2$O$_3$ with that of the corresponding experimental spectrum.

Theoretical spectra of two reference compounds, i.e., $\alpha$-Al$_2$O$_3$ and ZnAl$_2$O$_4$, reproduce the experimental spectral shape as well as relative peak energies satisfactorily. In the experimental spectrum of the 19 at. % Al sample, the presence of three peaks, A, B, and C, can be clearly noted. The peak positions are indicated by hatched bands on the theoretical spectra in Fig. 14. The relative energy of the highest peak, B, is best reproduced by the homologous model. Peak C is well reproduced as well. The position of peak A is overestimated by 1.5 eV in the theoretical spectrum of the homologous model. This can be well explained by the superposition of small amount of Al with Zn-vacancy model which shows lower onset energy than the homologous model.

By comparison of the experimental spectrum with the theoretical fingerprints, the presence of Al with the local environment similar to the homologous model is implied. This is consistent with our interpretation for the *c* axis expansion and first principles energetics as discussed in previous sections. Because of low signal to background ratio in the experimental spectra from PLD films, as shown in Fig. 7, it is difficult to discuss the Al concentration dependence of the Al-*K* edge XANES at the present moment. However, more detailed XANES analysis of dependences on solute concentration, deposition conditions, and heat treatments with improved quality of signal should be very useful to reveal the evolution of the atomic structures in the supersaturated solid solutions.

## VI. SUMMARY

The atomic structures of supersaturated ZnO–Al$_2$O$_3$ (>20 at. % Al) thin films deposited by PLD on silica glass substrates at 600 °C have been investigated in detail. Major results can be summarized as follows:

(1) The solubility limit of Al in wurtzite ZnO in ceramic samples sintered at 1350 °C for 3 h is determined by combination of XRD and Al-*K* edge XANES. It is found to be lower than 3 at. %, which roughly agrees with literature.[20] ZnAl$_2$O$_4$ phase with a normal spinel structure is found to appear when the Al concentration is higher than the solubility limit in the ceramic samples.

(2) The PLD films are composed of textured wurtzite grains with *c* planes parallel to the glass substrate surface. The distance between *c* planes expands significantly when the Al concentration is greater than 10 at. %. The expansion disappears after annealing of the PLD films at above 800 °C.

(3) High density of dislocationlike atomic structures is found in the as deposited film by high resolution cross-sectional TEM. Any segregation of Al cannot be detected either at the grain boundaries or inside the grains using TEM-EDS with electron-beam spot-size of 1 nm.

(4) Systematic first principles calculations are made for simplified wurtzite ZnO:Al models with Al at the substitutional Zn site and a Zn vacancy (Zn-vacancy model). The expansion toward the *c* axis cannot be explained by these models. Alternatively, a homologous model with the composition of (ZnO)$_3$(Al$_2$O$_3$) is made from the analogy to the ZnO–In$_2$O$_3$ system. Al atoms in this model are CN=4, 5, and 6, which is in contrast to the Zn-vacancy model with only Al atoms of CN=4. The interplanar distance between *c* planes can be well explained using the homologous model.

(5) First principles calculations show that the homologous structure is energetically more favorable than the Zn-vacancy model, although decomposition into ZnO and ZnAl$_2$O$_4$ is more favorable than the homologous structure. The homologous structure may therefore be metastable.

(6) First principles calculations of Al-*K* edge XANES of different phases are made using supercells composed of more than 100 atoms and a core-holed Al atom. Comparison between experimental and theoretical spectra implies that the supersaturated solid solution is composed of Al atoms with local atomic structures similar to the homologous phase.

In conclusion, all of experimental data for the supersaturated ZnO–Al$_2$O$_3$ solid solutions can be consistently explained by taking the homologous model as the local structure of Al.

[1] N. Nadaud, N. Lequeux, N. Nanot, J. Jove, and T. Roisnel, J. Solid State Chem. **135**, 140 (1998).
[2] R. Wang, A. W. Sleight, and D. Cleary, Chem. Mater. **8**, 433 (1996).
[3] N. Roberts, R. P. Wang, A. W. Sleight, and W. W. Warren, Jr., Phys. Rev. B **57**, 5734 (1998).
[4] I. Tanaka and H. Adachi, Phys. Rev. B **54**, 4604 (1996).
[5] T. Mizoguchi, I. Tanaka, M. Yoshiya, F. Oba, K. Ogasawara, and H. Adachi, Phys. Rev. B **61**, 2180 (2000).
[6] I. Tanaka, T. Mizoguchi, T. Sekine, H. He, K. Kimoto, T. Kobayashi, S. D. Mo, and W. Y. Ching, Appl. Phys. Lett. **78**, 2134 (2001).
[7] T. Mizoguchi, I. Tanaka, M. Kunisu, M. Yoshiya, H. Adachi, and W. Y. Ching, Micron **34**, 249 (2003).
[8] T. Mizoguchi, I. Tanaka, S. Yoshioka, M. Kunisu, T. Yamamoto, and W. Y. Ching, Phys. Rev. B **70**, 045103 (2004).

[9]K. Tatsumi, T. Mizoguchi, S. Yoshioka, T. Yamamoto, T. Suga, T. Sekine, and I. Tanaka, Phys. Rev. B **71**, 033202 (2005).

[10]A. Suzuki, T. Matsushita, N. Wada, Y. Sakamoto, and M. Okuda, Jpn. J. Appl. Phys., Part 2 **35**, L56 (1996).

[11]S. M. Park, T. Ikegami, and K. Ebihara, Jpn. J. Appl. Phys., Part 1 **44**, 8027 (2005).

[12]S. Choopun, R. D. Vispute, W. Yang, R. P. Sharma, T. Venkatesan, and H. Shen, Appl. Phys. Lett. **80**, 1529 (2002).

[13]E. Tegeler, N. Kosuch, G. Wiech, and A. Faessler, Phys. Status Solidi B **84**, 561 (1977).

[14]P. E. Blöchl, Phys. Rev. B **50**, 17953 (1994).

[15]G. Kresse and J. Furthmüller, Phys. Rev. B **54**, 11169 (1996).

[16]J. P. Perdew, K. Burke, and M. Ernzerhof, Phys. Rev. Lett. **77**, 3865 (1996).

[17]H. J. Monkhorst and J. D. Pack, Phys. Rev. B **13**, 5188 (1976).

[18]P. Blaha, K. Schwarz, G. Madsen, D. Kwasicka, and J. Luitz, WIEN2K, an augmeted plane wave+local orbitals program for calculating crystal properties ISBN 3-9501031-1-2. Karlheinz Schwarz, Techn. Universitat Wien, Austria, 2001.

[19]I. Tanaka, T. Mizoguchi, and T. Yamamoto, J. Am. Ceram. Soc. **88**, 2013 (2005).

[20]M. H. Yoon, S. H. Lee, H. L. Park, H. K. Kim, and M. S. Jang, J. Mater. Sci. Lett. **21**, 1703 (2002).

[21]F. Oba, H. Ohta, Y. Sato, H. Hosono, T. Yamamoto, and Y. Ikuhara, Phys. Rev. B **70**, 125415 (2004).

[22]JCPDS File No. 36-1451; JCPDS File No. 05-0664.

[23]A. Savitzky and M. J. E. Golay, Anal. Chem. **36**, 1627 (1964).

[24]J. Mass, P. Hattacharya, and R. S. Katiyar, Mater. Sci. Eng., B **103**, 9 (2003).

[25]H. Kasper and Z. Anorg, Z. Anorg. Allg. Chem. **349**, 113 (1967).

[26]N. Kimizuka, M. Isobe, and M. Nakamura, J. Solid State Chem. **116**, 170 (1995).

[27]C. Li, Y. Bando, M. Nakamura, and N. Kimizuka, J. Electron Microsc. **46**, 119 (1997).

[28]C. Li, Y. Bando, M. Nakamura, and N. Kimizuka, Acta Crystallogr., Sect. B: Struct. Sci. **55**, 355 (1999).

[29]W. Pitschke and K. Koumoto, Powder Diffr. **14**, 213 (1999).

[30]C. Schinzer, F. Heyd, and S. F. Matar, J. Mater. Chem. **9**, 1569 (1999).